The Impact of Realistic Footprint Shapes on the Connectivity of Wireless Sensor Networks

Flavio Fabbri
WiLab, DEIS, University of Bologna
V.le Risorgimento, 2
I-40136 Bologna, Italy
flavio.fabbri@unibo.it

Cengiz Gezer
WiLab, DEIS, University of Bologna
V.le Risorgimento, 2
I-40136 Bologna, Italy
cengiz.gezer@unibo.it

Roberto Verdone
WiLab, DEIS, University of Bologna
V.le Risorgimento, 2
I-40136 Bologna, Italy
roberto.verdone@unibo.it

ABSTRACT

Radio channel fluctuations affecting links of Wireless Sensor Networks (WSNs) show an evident spatial correlation, besides the random behavior caused by obstacles and fading effects. This makes node footprints (i.e. the area covered by the radio transmitter of a node) irregular. Nonetheless, the vast majority of models used in the literature to assess the performance of WSNs in terms of network connectivity, neglect this evidence. They usually consider either the deterministic disk model (with circular footprints) or some random connection model assuming i.i.d. channel fluctuations when different links are realized at the same node with different neighbors.

We show in this paper that in realistic settings the spatial correlations of the random fluctuations play a relevant role; we support this statement with an analysis starting from real measurements performed on-field. However, we also show that the i.i.d model provides results which can be close enough to reality in some cases.

More precisely, assuming a constant average number of neighbors, we study the percolating properties of realistic and theoretical footprints on random graphs by computing the relative size of the largest component of the graph. Our results show that the presence of correlation may be beneficial or detrimental, depending of whether one considers undirected or directed graphs, i.e., ultimately, on the application.

1. INTRODUCTION

Wireless ad-hoc and sensor networks are proven to be a rich field of investigation [2]. The great majority of such networks exploit multi-hopping techniques to route information along and, for this reason, they require a high degree of connectivity.

Many works devoted their attention to connectivity issues of wireless networks both from a very theoretical perspective (e.g. using percolation theory, graph theory, geometric probability [1,6,9,18]) and experimentally [10]. The analysis of wireless networks connectivity based on solid mathematical ground as well as on computer simulation brought to light how performance strongly depends on the way links from node to node are modeled [7]. Early connectivity papers (see, e.g., [19]) extensively employed the disk model (i.e., assumed a node has connections to all nodes within a fixed Euclidean distance) because of its simplicity and analytical tractability. Pioneering results were achieved in that fashion. However, by looking at the coverage area of the transceiver (also denoted here as footprint) of any commercial platform in realistic environments ([13], Figure 1), one can figure out that reality is way more complex, due to a variety of physical phenomena (presence of intra-nodal obstructions, scatterers, etc...) poorly captured by the disk model.

Probabilistic tools revealed to be more adequate for modeling unstable and fluctuating links in wireless networks. Owing to this motivation, the Random Connection Model (RCM) [12], which assigns a link between two nodes with some probability (depending, e.g., on their distance), has been increasingly used [3, 4, 14, 15, 20]. The RCM as described, e.g., in [7], gives rise to a graph where the edges are set by "throwing a dice" for every pair of nodes. In other words, even if it accounts for channel randomness, it assumes independence from link to link. This implies that neighboring links can potentially experience similar as well as dramatically different fluctuations with the same probability. However this conclusion is not supported by experimental evidence which, rather, clearly shows spatial correlated channel fluctuations, where the amount of correlation depends on the environment [13].

That said, we intuitively believe that neither RCMs nor disk models (which are two extreme opposites) reflect the reality and we support such intuition by means of real measurements. However, the final outcome of our experiments suggests that RCM is much more realistic than its counterpart. In this paper we also fill the gap between the two mentioned models by proposing a Correlated Random Connection Model (CRCM) which accounts for the angular correlation of the channel fluctuations by means of tunable parameter, α. Hence, α controls the severity of correlation and ranges from zero to infinity. When it reaches zero (infinity), our model degenerates to the traditional disk model (RCM).

As starting point, we consider a previously adopted statistical link model [15], which determines when one node is "audible" to another node, and we generalize it to handle

WSNPERF 2009, October 23, Pisa, Italy

DOI10.4108/ICST.VALUETOOLS2009.7770

the case of exponentially correlated fluctuations. The exponential law is chosen for its simplicity, since no other consolidated correlation function is found in the literature for this matter. Moreover, we explore the percolating properties of the CRCM on the random graph when varying α and compare it to some reference cases of both theoretical and practical flavor. In particular, we also present the results of a measurement campaign devoted to showing how fluctuations vary as function of the angle and use such results as benchmark. We then study the percolation properties of this model, meaning that we examine the behavior of nodes clusters arisen in the graph when applying such a link model to every pair of nodes in the network. Our performance metrics is the relative size of the largest component of the graph.

The analysis focuses on two types of graph, directed and undirected. From graph theory, a graph is undirected when for each pair of vertices A and B, the costs of arcs from A to B and from B to A are the same in both directions. In the other case it is said to be directed. In our case we consider the cost to be 0 when, say, A has a connection to B and infinite when no such path exists. Therefore when a communication graph is undirected we either have a bidirectional A-B connection or we don't have it at all (i.e., the cost is infinite). Such a distinction is not imposed but rather descends from not just considering centrally symmetric footprint shapes [6]. In the case of *directed* graphs we consider two nodes to be connected if either of them is audible to the other. The results show in this case that the presence of correlation is detrimental from the network connectivity viewpoint. In the case of *undirected* graphs instead we consider two nodes to be connected if both of them are audible to the other. It appears that in this case correlation is beneficial to network connectivity.

The rest of the paper is articulated as follows. In Section 2, related works are presented and the main contact points/differences with the present work are underlined. Section 3 introduces a statistical link model from the literature. Section 4 presents our correlated random connection model. Our experimental measurements are described in Section 5. Finally Sections 6 and 7 reports numerical results and conclusions, respectively.

2. RELATED WORKS

This paper is largely based on the work done by Franceschetti *et al.* in [6], where the percolating properties of random graphs under various connections models are addressed. The simulations are performed with the underlying assumption of considering only bidirectional links: this is made possible by the exploitation of *centrally symmetric shapes* all deployed on the nodes with the same orientation angle, which ensure that if a node falls into the footprint of another node, the reverse is also true. While preserving the approach of [6], we relax this constraint by considering both non centrally symmetric shapes and their deployment with random orientation angles. As a consequence, we also treat the case of non reciprocal links and the distinction between directed and undirected graphs arises from here. The properties of random connection models (see [7, 12]) are also explored in [6]. However the traditional RCM does not allow to account for the correlation experienced by those links sharing one of the two endpoints, which rather constitutes a physical evidence.

In [17] and [16] the Authors state they are the first to address the effects of correlated shadowing on the connectivity of ad-hoc networks, and introduce *NeSh*, a joint shadowing model for links formation in a multi-hop network. According to NeSh, the random component of the power loss (in dB scale) at the receiver of node j when node i is transmitting, is split into the sum of two contributions: the shadowing loss and the non-shadow fading loss. The shadowing loss is assumed to have some spatial correlation.The main strength of this model is the possibility to account for correlation between any two pair of links, no matter if they share some endpoint or not. Instead, in the present paper we only focus on correlation which affects two links sharing one endpoint. However, one drawback of NeSh is that it only generates one shadowing sample per link, thus indirectly assuming that links experience the same channel fluctuation in both directions. This might be reasonable when modeling some large-scale phenomenon (e.g., the effect of an obstruction), while it is not the case of more general channel fluctuations found in ad-hoc and WSNs, where large and small scale contributions are almost undistinguishable due to the small distances [20]. Hence, while we share with [16, 17] the argument that the reality lies in between the disk and the i.i.d. channel fluctuation models, we adopt a different approach and, indeed, also reach a different conclusion: unlike stated in [16], we show that it is not necessarily true that i.i.d. link fading models lead to an overestimation of network connectivity.

[11] is devoted to the effects of cross-correlated shadowing in the simulation of cellular networks. Even though we are more on infrastructure-less networks, we follow the same strategy for generating correlated Gaussian random variables (r.v.'s), that is via the *Cholesky factorization* of the correlation matrix.

3. THE LINK MODEL

We make extensive use of the concept of "*footprint*": the footprint of a node i is the 2D-region $\mathfrak{F}_i$ such that a direct edge connecting i to a potential node j can be drawn in the graph if and only if j is in $\mathfrak{F}_i$, where we assume that the presence of a link is the binary quantization of some physical parameter (e.g., the received power). How a footprint looks like is dictated by the link model employed. However, the key fact to keep in mind is that, when dealing with a statistical link model (as done here), the footprint is itself a statistical object. Therefore, we will sometimes denote as "realization of footprint" a particular outcome of the corresponding random process generating it. Unless otherwise stated, the expected area of the footprint is kept constant, while we study the impact of changing its shape.

A link model that shows good adherence to the physical world of wireless networks is adopted in [15]. It accounts for the power loss due to propagation effects including both a distance-dependent path loss and random channel fluctuations caused by possible obstructions. Specifically, a directed radio link between two nodes is said to exist if $L < L_{\text{th}}$, where L is the power loss and L_{th} represents the maximum loss tolerable by the communication system. In that case, one node is said to be "*audible*" by the other. The threshold L_{th} depends on the transmit power and the receiver sensitivity. The power loss in decibel scale at distance d is expressed in the following form

$$L = k_0 + k_1 \ln d + s, \tag{1}$$

where k_0 and k_1 are constants, s is a Gaussian r.v. with zero mean, variance σ^2, which represents the channel fluc-

Digital Object Identifier: 10.4108/ICST.VALUETOOLS2009.7770
http://dx.doi.org/10.4108/ICST.VALUETOOLS2009.7770

tuations. By suitably setting k_1, it is possible to accommodate an inverse square law relationship between power and distance ($k_1 = 8.69$), or an inverse fourth-power law ($k_1 = 17.37$), as examples. This can be viewed as a RCM which assign a directed link between two nodes at distance x with probability

$$g(x) = 1 - \frac{1}{2}\text{erfc}\left(\frac{L_{\text{th}} - k_0 - k_1 \log x}{\sqrt{2}\sigma}\right). \quad (2)$$

By solving (1) for the distance d with $L = L_{\text{th}}$, we can define the transmission range $TR = e^{\frac{L_{\text{th}} - k_0 - s}{k_1}}$ as the maximum distance between two nodes at which communication can still take place.

TR defines the footprint of a node. However, independent r.v.'s s for separate links are adopted, resulting in different values of TR in each direction, given a generic node. This yields a highly "jagged" footprint (similar to that of Figure 2, top-right).

4. A CORRELATED RANDOM CONNECTION MODEL (CRCM)

We report here for the sake of completeness the model description as can be also found in [5]. Assuming three nodes, A, B_1, B_2, are arbitrarily placed on a plane as in Figure 1(a), we focus on the two events of node A being audible to both nodes B_1 and B_2. By employing the link model described in Section 3 and letting $d(\cdot,\cdot)$ denote the Euclidean distance operator, the channel losses (in dB scale) from A to B_1 and from A to B_2 are (from (1))

$$L(A, B_i) = k_0 + k_1 \ln d(A, B_i) + \mathbf{S}(\theta_i), \quad i = 1, 2, \quad (3)$$

where $\mathbf{S}(\theta)$ is a continuous stationary Gaussian random process having mean $E[\mathbf{S}(\theta)] = 0$ and autocorrelation

$$R_S(\phi) = \sigma^2 e^{-\alpha|\phi|}, \quad \phi \in [-\pi, \pi], \quad (4)$$

with σ^2 being constant and $\alpha \in [0, +\infty[$ a tunable parameter. As a consequence, $\mathbf{S}(\theta_1)$ and $\mathbf{S}(\theta_2)$ are jointly Gaussian with zero mean and covariance matrix

$$\Sigma = \sigma^2 \begin{bmatrix} 1 & \rho_{1,2} \\ \rho_{1,2} & 1 \end{bmatrix}, \quad (5)$$

with $\rho_{1,2} = e^{-\alpha|\theta_2 - \theta_1|}$. Practically speaking, unlike the case where we employ the traditional RCM, here the channel fluctuations that affect the communications from A to B_1 and from A to B_2 are correlated by means of an exponentially decaying law. The parameter α may be set in such a way to strengthen or loosen the angular correlation distance. For instance, we may want $R_S(\phi)$ to be less then ϵ for some angle ϕ^*: in this case we need to set $\alpha > -\frac{\ln(\epsilon/\sigma^2)}{|\phi^*|}$. When $\alpha \to \infty$, $\mathbf{S}(\theta)$ simply becomes white Gaussian noise and the usual uncorrelated RCM is found.

Now imagine that nodes B_1 and B_2 can move along the straight lines intersecting in A. The maximum distances at which communication can take place are (from (3))

$$\mathbf{R}(\theta_i) = e^{\frac{L_{\text{th}} - k_0 - \mathbf{S}(\theta_i)}{k_1}}, \quad i = 1, 2 \quad (6)$$

where L_{th} is the maximum loss tolerated by the system. $\mathbf{R}(\theta_1)$ and $\mathbf{R}(\theta_2)$ are two r.v.'s themselves.

If we now generalize Figure 1(a) and assume there are N receiving nodes $B_1, \ldots, B_N$ equally distributed on the full

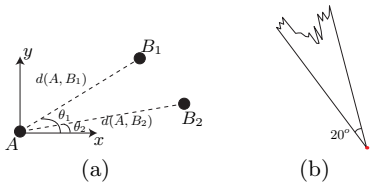

Figure 1: (a): Reference scenario for the introduction of CRCM. (b): Realization of a slice.

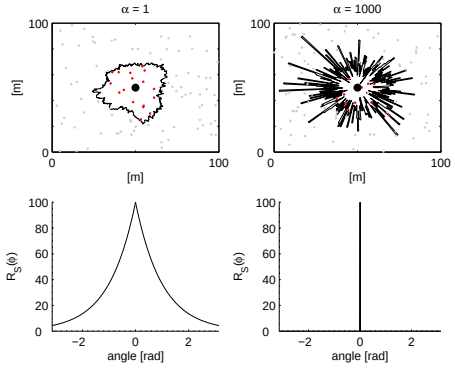

Figure 2: Top: two realizations of footprints obtained with $\alpha = 1$ and $\alpha = 1000$, respectively, and $\sigma = 10$, $L_{\text{th}} = 32.32$ dB, $k_0 = 40$, $k_1 = 13.03$. Bottom: corresponding autocorrelation functions, $R_S(\phi)$, of the gaussian fluctuations.

circle (i.e., each one at angular distance $\Delta\theta = 2\pi/N$ from the neighbor), the r.v.'s $\mathbf{R}(\theta_i) = \exp\left((L_{\text{th}} - k_0 - \mathbf{S}(\theta_i))/k_1\right)$, $i = 1, \ldots, N$, define the maximum communication distance for the directions $\theta_1, \ldots, \theta_N$ (see [5], Appendix for implementation details). Now by letting $N \to \infty$ we end up with the random process

$$\mathbf{R}(\theta) = \exp\left((L_{\text{th}} - k_0 - \mathbf{S}(\theta))/k_1\right) = r_0 \exp(-\mathbf{S}(\theta))/k_1), \quad (7)$$

with $r_0 = \exp\left((L_{\text{th}} - k_0)/k_1\right)$, which defines the maximum communication distance in each direction, that is, the footprint of node A. Two realizations of footprint are reported in Figure 2 together with the corresponding function $R_S(\phi)$, for $\alpha = 1, 1000$ and $\sigma = 10$. Note how the shape is more regular when $\alpha = 1$ while appears incoherent for $\alpha = 1000$. The expected area of a footprint does not depend on α and may be computed as

$$E[A] = E\left[\frac{1}{2}\int_0^{2\pi} \mathbf{R}^2(\theta) d\theta\right] = \frac{1}{2}\int_0^{2\pi} E[\mathbf{R}^2(\theta)] d\theta \quad (8)$$

$$= \frac{r_0^2}{2}\int_0^{2\pi} E[e^{-2\mathbf{S}^2(\theta)/k_1}] d\theta. \quad (9)$$

By noting that $e^{-2\mathbf{S}^2(\theta)/k_1}$ of (9) is Log-N$(0, 4\sigma^2/k_1^2)$, we easily find $E[A] = \pi r_0^2 e^{2\sigma^2/k_1^2}$.

5. EMPIRICAL FOOTPRINT ESTIMATION

We describe here our measurement campaign conducted in order to experimentally estimate the footprint of a node.

Digital Object Identifier: 10.4108/ICST.VALUETOOLS2009.7770
http://dx.doi.org/10.4108/ICST.VALUETOOLS2009.7770

5.1 Experimental Setup

A series of measurements have been conducted in an outdoor area located in the campus of engineering department at University of Bologna. During the experiments a floating transmitter sends data packets to a fixed receiver from different angles and distances. The measurements take place over a grass terrain which is not perfectly flat and grass growing is not homogenous. However, no object is present in the vicinity (within a 30 meters radius) which may cause significant reflection besides few trees. Transmitter is positioned 2 and 3 meters away from the receiver at 0, 45, 60, 70, 80, 90, 100, 110, 120, 135, 180, and 270 degrees with respect to a fixed point (see Figure 3). A rope and a A4 size protractor has been used to point out the measurement angles. The orientation of the receiver is never changed during the experiment, while the transmitter at each angle is rotated in such a way to always face the location of the receiver with the same side.

We took two distinct measurement campaigns. In the first one both devices are at 15 cm above ground placed on two paperboard boxes. In the second one, transmitter and receiver are deployed directly on the grass.

The devices employed for the experiments are Freescale 1322x-USB and Freescale 1322x-LPB [8] (see Figure 4), used as receiver and transmitter, respectively. Such development boards are based on Freescale MC13224V Platform, which is 802.15.4 compatible, and work on the 2.4 GHz band. The typical receiver sensitivity is -95 dBm and the transmit power is set to the default value of 0 dBm. We also report as example the antenna beam pattern on the XY plane (i.e., that one of interest to our experiments) for the 1322x-LPB device in Figure 5. Even though it looks roughly isotropic (at least for the vertical polarization), it should be considered that the joint radiation pattern (i.e., antenna + board) will be somewhat different. The same holds for 1322x-USB. Transmitter sends 20 bytes long PHY Protocol Data Units (PPDU) in 30 msec intervals and receiver, upon reception of each packet, is able to estimate the receiving power associated to that packet. We emphasize that there is no 802.11 access point close enough to drastically influence link quality.

In Figure 6 we report, as example, the average received power at 2 meters distance in dBm as a function of the angle, in the case where both devices are placed on boxes. The average is computed over 10000 received packets and standard deviation is also reported in the error bars. As one can see, the received power is highly variable depending on the angle. This is due to several concurrent phenomena. In particular, at each angle the radio channel has different characteristics because of the presence of obstructions and reflection of the ground. Moreover, the different relative orientation of the two beam patterns at each angle may either penalize or favor the amount of received power in a random manner.

5.2 Estimation Procedure

Once we have collected received power values at 2 and 3 meters distance for the above mentioned angles, we can easily construct an approximation of the channel loss $\hat{L}(d,\theta_i) = \hat{k}_0(\theta_i) + \hat{k}_1(\theta_i)\ln d$, with θ_i belonging to the set of observed angles, by estimating the parameters k_0 and k_1 from the experimental values.

To this end, by suppressing for simplicity the dependence of k_0 and k_1 on the angle, we have for each θ_i the linear

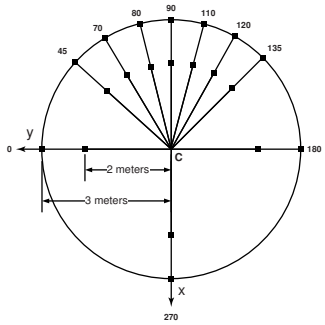

Figure 3: Sketch of the experimental setup: receiver is located in the circle center (C) and transmitter in all the positions marked with a square.

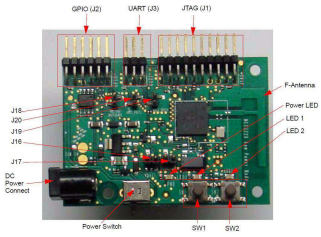

(a)

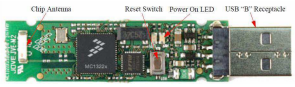

(b)

Figure 4: (a) Freescale 1322x-USB. (b) Freescale 1322x-LPB.

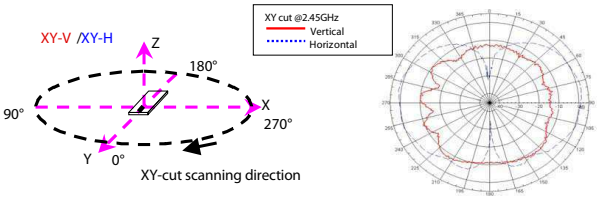

Figure 5: Antenna beam pattern on the XY plane for the Freescale 1322x-LPB device.

system

$$\begin{cases} P_{\mathrm{r}}(d_1) &= P_{\mathrm{T}} - \hat{k}_0 - \hat{k}_1 \ln d_1 \\ P_{\mathrm{r}}(d_2) &= P_{\mathrm{T}} - \hat{k}_0 - \hat{k}_1 \ln d_2 \end{cases}, \qquad (10)$$

where $P_{\mathrm{r}}(x)$ is the received power at distance x, $P_{\mathrm{T}} = 0$ dBm is the transmitting power, $d_1 = 2$ [m] and $d_2 = 3$ [m], which can be solved to find $\hat{k}_0$ and $\hat{k}_1$.

Once $\hat{k}_0(\theta_i)$ and $\hat{k}_1(\theta_i)$ are known, the estimated foot-

Digital Object Identifier: 10.4108/ICST.VALUETOOLS2009.7770
http://dx.doi.org/10.4108/ICST.VALUETOOLS2009.7770

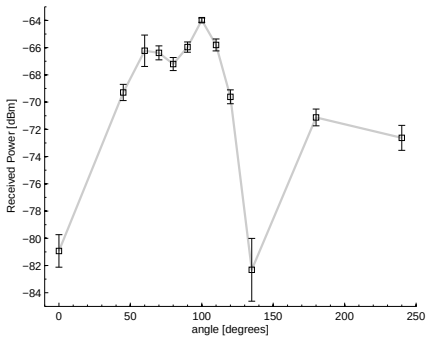

Figure 6: Average received power in the experimental setup with transmitting and receiving nodes 2 meters far apart both at 15 cm above ground.

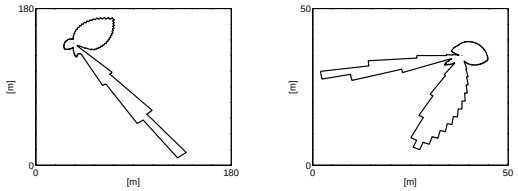

(a) (b)

Figure 7: Footprint sample estimated by measured data in the case where transmitting and receiving nodes are placed (a) 15 cm above ground and (b) on the grass.

print in the direction θ_i is simply the distance R such that $\hat{L}(R, \theta_i) = L_{\text{th}}$, i.e.,

$$R(\theta_i) = e^{\frac{L_{\text{th}} - \hat{k}_0(\theta_i)}{k_1(\theta_i)}}, \tag{11}$$

with $L_{\text{th}} = 95$ dB. Then, the extension to a generic $\theta \in [0, 2\pi]$ is obtained by linear interpolation.

In Figure 7 we report the footprints obtained through our measurement campaign for the two cases where devices are placed on boxes and where they are on the grass. First, both sketches reveal quite irregular shapes with a low degree of angular correlation and potentially large deviations. The reason of this is once again to be found in different propagating conditions at each angle as well as in the possible alignment of minima and maxima of the two radiating patterns. Notice also the scale is not the same in Figures 7(a) and 7(b): the patter in 7(a) covers a larger area than the one in 7(b). This is in accordance with the fact that the first one is obtained with elevated devices (which are less affected by grass obstruction).

6. NUMERICAL RESULTS

Here we explore the percolating properties of the CRCM introduced in Section 4 as well as those of the empirical shapes derived in Section 5. Recalling (9), we remarked that the expected area, $E[A]$, of the footprint does not vary with α: this is of primary importance toward our goal. In fact, when nodes are distributed on the plane according to a stationary Poisson Point Process, the number of neighbors of a given node is Poisson distributed with mean given by the nodes density times $E[A]$. This fact allows us to merely evaluate the effects of differently shaped footprints on network percolation, while keeping a constant average number of neighbors. Moreover, in order to make a fair comparison, we also normalize the two experimental footprints in such a way that they have equal area and that it is also equal to the mean area of probabilistic footprints.

Each point in the plots shown in Figs. 8 and 9 has been obtained by means of 500 simulation runs. At each run, 500 nodes (on average) are randomly distributed on a square region of side $L = \sqrt{500/\lambda}$, with λ being the nodes density. For the probabilistic footprint case, a total number, n_f, of realizations of footprints are generated and normalized so that they all have the same area, and each node gets a shape assigned at random. When instead we employ experimental footprints, we use only one of the shapes at a time and assign it to each node with different (random) orientation. In particular, in the following figures "footprint 1" is the one derived by placing the devices at 15 cm above ground, while "footprint 2" is the one where the devices lie on the grass. Based on the topology created, the adjacency matrix is computed and the properties of the graph are evaluated. We focus especially on the relative size of the largest component.

In Figure 8 the relative size of the largest component for *directed* graphs is reported as a function of the nodes density. The four solid lines without markers represent the cases of angularly correlated footprints, with $\alpha = 0, 1, 2, \infty$. Recall that $\alpha = 0$ and $\alpha = \infty$ are two boundary situations, since the former represents circular footprints while the latter gives rise to completely uncorrelated fluctuations. It clearly appears that the more they are uncorrelated (larger α), the smaller is the percolating density threshold. The reason of this is that more incoherent shapes, once the area is fixed, tend to spread further. As a consequence, while the number of neighbors of a node remains the same, their distance distribution has a heavier tail and this seems to help percolation. On the contrary, circles tend to let the neighbors "clusterize" in the vicinity of a node. To emphasize this, we also propose a purely theoretical comparison with non-probabilistic footprints, namely squares and triangles. Both of them perform better than circles: in fact, it is easy to figure out that shapes having fewer angles keep neighbors farther with respect to circles of the same area. Taking this argument to the extreme, we consider "slices", which are circular sectors of angle $\beta = 20^o$ and fluctuating border (see Figure 1(b)). They somehow resemble the radiation pattern of a directional antenna and allow neighbors to be even farther, thus being the shape percolating at the lowest density. We thus conclude that correlation is a penalizing fact in directed graphs. Finally, the two solid curves with markers are obtained by means of the measured footprints. We clearly notice that both of them are on the left side of the plot, meaning that their behavior is very close to that of theoretical curves obtained with a low degree of correlation and quite far from that of circles.

In Figure 9 the relative size of the largest component for *undirected* graphs is reported as function of nodes density. The first thing to note is that the density scale is stretched out and percolation happens at larger density values for all curves, with respect to Figure 8. This is explained as fol-

Digital Object Identifier: 10.4108/ICST.VALUETOOLS2009.7770
http://dx.doi.org/10.4108/ICST.VALUETOOLS2009.7770

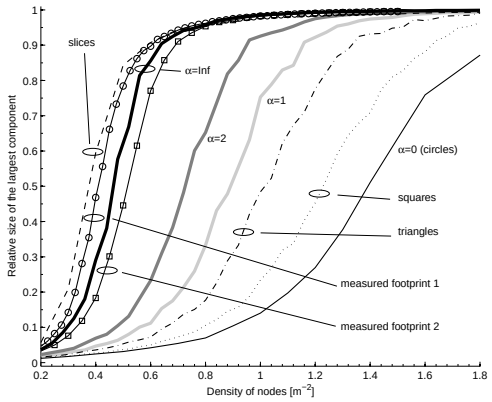

Figure 8: Directed graphs: relative size of the largest component as function of nodes density, obtained with different footprints all having $E[A] = \pi$, $N = 100$ angular samples. $n_f = 10$ for probabilistic ones.

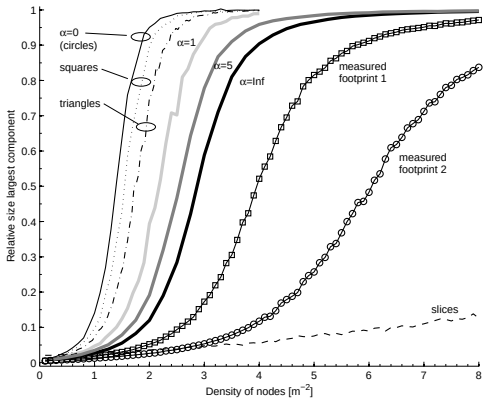

Figure 9: Undirected graphs: relative size of the largest component as function of nodes density, obtained with different footprints all having $E[A] = \pi$, $N = 100$ angular samples. $n_f = 10$ for probabilistic ones.

lows: now an edge connecting to vertices is drawn in the graph only if the two nodes are both in each other's footprint. This happens with a smaller probability compared to the event of having either one of the nodes in each other's footprint. The second, less trivial, issue which can be observed in the plot is that the trend is inverted, meaning that in this case correlation is beneficial to network connectivity. In particular, circles result to be the most easily percolating shape, while slices are at the opposite extreme. The reason of this is the following: if a node A is audible to a node B at large distance, owing to a maximum of the footprint of B in the direction of A, reciprocity would require the footprint of A to have a maximum of the same size (or greater) exactly in the direction of B. This is of course an extremely rare event. Instead, considering footprints which are quite regular when the angle varies, if the event "A audible to B" is verified, the reverse is very likely to hold, too. At the extreme, when circles are considered, the reverse is *necessarily* true. Finally, the curves obtained with measured footprints are once again very far from the case of circles and most regular shapes. It is also worth noting that they are quite far from each other although based on footprints that were obtained in similar experimental conditions. The reason is that the footprint of Figure 7(a) exhibits only one major lobe which makes it look more like a "slice", while the other one (Figure 7(b)) has two equally relevant lobes: having two directions of maxima instead of one greatly enhances the probability of connection in undirected graph scenario.

7. CONCLUSIONS

In this paper we have introduced a simple model for taking into account the correlation of the fluctuations affecting radio links in WSNs (the considerations also hold for ad-hoc networks). The degree of such correlations has been modeled by means of a tunable parameter. For some setups our model degenerates into previously introduced ones, namely the disk model and the i.i.d. fluctuations model, which have been shown to be boundary cases. Percolation of correlated footprints on the random graph has been studied in the two cases of directed and undirected graphs, and comparisons to non-probabilistic footprints have been provided. The study has revealed that correlations of channel fluctuations are beneficial in directed graphs while they are detrimental in undirected ones. Hence, their effects can only be evaluated within specific application contexts, while no general trend is observed.

Moreover, we have presented the results of our experimental campaign and used them as a benchmark. From the comparison, we showed that neither i.i.d. models nor disk-like ones can claim to be accurate enough. However, we have also learnt that connectivity in real life WSNs is better captured by uncorrelated RCMs models.

8. ACKNOWLEDGMENTS

The authors wish to thank Mirco Sapucci for the help provided in the experimental activity.

9. REFERENCES

[1] C. Bettstetter. On the minimum node degree and connectivity of a wireless multihop network. In *Mobile Ad Hoc Networks and Comp.(Mobihoc), Proc. ACM Symp. on*, June 2002.

[2] D. Culler, D. Estrin, and M. Srivastava. Overview of sensor networks. 37(8):41–49, Aug. 2004.

[3] F. Fabbri and R. Verdone. A multi-sink multi-hop wireless sensor network over a square region: Connectivity and energy consumption issues. In *IEEE GLOBECOM 2008 Workshops, accepted*, 30 Nov-4 Dec 2008.

[4] F. Fabbri and R. Verdone. A statistical model for the connectivity of nodes in a multi-sink wireless sensor network over a bounded region. In *IEEE 14th European Wireless Conference, EW2008*, pages 1–6, 22-25 Jun 2008.

[5] F. Fabbri and R. Verdone. The impact of correlated channel fluctuations on the connectivity of wireless

Digital Object Identifier: 10.4108/ICST.VALUETOOLS2009.7770
http://dx.doi.org/10.4108/ICST.VALUETOOLS2009.7770

ad-hoc networks. In *IEEE 69th Vehicular Technology Conference (VTC-spring 2009), Apr 26-29th, Barcelona, Spain*, 2009.

[6] M. Franceschetti, L. Booth, M. Cook, R. Meester, and J. Bruck. Continuum percolation with unreliable and spread-out connections. *Journal of Statistical Physics*, 118(3/4):721–734, Feb. 2005.

[7] M. Franceschetti and R. Meester. *Random Networks for Communication: From Statistical Physics to Information Systems*. 2007.

[8] Freescale Semiconductor. 1322x development kits. Datasheet available on `http://www.freescale.com/webapp/sps/site/prod_summary.jsp?code=1322x_Dev_Kits&parentCode=MC13224V`.

[9] P. Gupta and P. Kumar. Critical power for asymptotic connectivity. In *Proc. of the 37th IEEE Conference on Decision and Control*, Tampa, Florida, USA, Dec. 1998.

[10] J. Kazemitabar, H. Yousefi'zadeh, and H. Jafarkhani. The impacts of physical layer parameters on the connectivity of ad-hoc networks. In *IEEE International Conference on Communications 2006*, volume 4, pages 1891–1896, 2006.

[11] T. Klingenbrunn and P. Mogensen. Modelling cross-correlated shadowing in network simulations. In *Vehicular Technology Conference, VTC - Fall. IEEE VTS 50th*, volume 3, pages 1407–1411, 19-22 Sept. 1999.

[12] R. Meester and R. Roy. *Continuum Percolation*. 1996.

[13] E. Miluzzo, X. Zheng, K. Fodor, and A. T. Campbell. Radio characterization of 802.15.4 and its impact on the design of mobile sensor networks. In *5th European Conference on Wireless Sensor Networks, EWSN'08, Bologna, Italy*, volume 1, pages 171–188, 2008.

[14] D. Miorandi and E. Altman. Coverage and connectivity of ad hoc networks presence of channel randomness. In *24th Annual Joint Conference of the IEEE Computer and Communications Societies, INFOCOM 2005.*, volume 1, pages 491–502, 2005.

[15] J. Orriss and S. K. Barton. Probability distributions for the number of radio transceivers which can communicate with one another. 51(4):676–681, Apr. 2003.

[16] N. Patwari and P. Agrawal. Effects of correlated shadowing: Connectivity, localization, and rf tomography. In *International Conference on Information Processing in Sensor Networks, IPSN*, pages 82–93, 22-24 April 2008.

[17] N. Patwari and P. Agrawal. Nesh: A joint shadowing model for links in a multi-hop network. In *IEEE International Conference on Acoustics, Speech and Signal Processing, ICASSP*, pages 2873–2876, March 31-April 4 2008.

[18] M. D. Penrose. On k-connectivity for a geometric random graph. *Random Structures and Algorithms*, 15:145–164, 1999.

[19] P. Santi and D. M. Blough. The critical transmitting range for connectivity in sparse wireless ad hoc networks. 2(1):25–39, 2003.

[20] R. Verdone, D. Dardari, G. Mazzini, and A. Conti. *Wireless sensor and actuator networks*. 2008.

Digital Object Identifier: 10.4108/ICST.VALUETOOLS2009.7770
http://dx.doi.org/10.4108/ICST.VALUETOOLS2009.7770